Long-Term Trend and Decadal Variability of Persistence of Daily 500-mb Geopotential Height Anomalies during Boreal Winter

RUIQIANG DING AND JIANPING LI

State Key Laboratory of Numerical Modeling for Atmospheric Sciences, and Geophysical Fluid Dynamics (LASG), Institute of Atmospheric Physics, Chinese Academy of Sciences, Beijing, China

(Manuscript received 24 October 2008, in final form 27 April 2009)

ABSTRACT

An analysis has been made of the trend and decadal variability of persistence of daily 500-mb (hPa) geopotential height anomalies for the winter season. The persistence is measured based on autocorrelations at 1- and 5-day lags (denoted r_1 and r_5, respectively) and the effective time between independent samples T_0. The results from linear trend analysis show that there exist significant trends of persistence of daily 500-mb geopotential height anomalies in some regions of the world. The regions with a significant decreasing trend are found to be mainly located at mid–high latitudes of the Northern and Southern Hemispheres, while the regions with a significant increasing trend are mainly located in the tropical Pacific Ocean. For other variables including sea level pressure (SLP), 1000-mb height, and 200-mb height, the persistence of daily anomalies also exhibits similar trends in these regions. It is speculated that the enhanced baroclinicity and advection are possibly responsible for the significant downward trend of persistence mainly occurring in the southern and northern mid–high latitudes, while the increased coupling between the atmospheric circulation and sea surface temperature (SST) could contribute to the increase of persistence in the tropical Pacific. An empirical orthogonal function (EOF) analysis based on the 7-yr Gaussian low-pass-filtered series of winter season r_1 and r_5 of 500-mb height (linear trend removed before the low-pass filtering) is presented. The results suggest that there is prominent decadal variability of persistence in some regions of the Northern and Southern Hemispheres and tropics. When compared with r_1, r_5 has decadal variations with larger magnitude and larger spatial scale. It is found that the decadal variability of persistence is closely related to decadal fluctuations of large-scale atmospheric circulation patterns.

1. Introduction

The importance of short-term (day to day) persistence in weather prediction has been recognized for a long time. As the simplest method of forecasting the weather, persistence forecasting has a good skill for cases with a stable weather pattern. The relationship between persistence and numerical weather prediction has been investigated by Macdonald and Shapiro (1964), who found that forecasts are more accurate when persistence is high and vice versa. Tracton et al. (1989) showed that while the National Meteorological Center (NMC) model generally does better than persistence, the general behavior of the time series of forecast skill based on persistence is very similar to the evolution of the skill of the NMC model.

Given their importance, persistence statistics are of great interest to meteorologists. The geographical variations of the persistence of daily geopotential heights have been studied. Klein (1951) and Gutzler and Mo (1983) showed that the greatest persistence in the Northern Hemisphere is observed over the polar regions and the eastern portions of the Atlantic and Pacific Oceans, while the least persistence is found off the east coasts of Asia and America. Trenberth (1985) showed that the largest persistence values in the Southern Hemisphere are found over the Antarctic, in low latitudes, and across Australasia, while the lowest persistence values are found in the main storm track regions. Trenberth (1985) further compared the difference between the persistence distributions in the Northern Hemisphere and Southern Hemisphere and found that the overall

Corresponding author address: Ruiqiang Ding, State Key Laboratory of Numerical Modeling for Atmospheric Sciences, and Geophysical Fluid Dynamics (LASG), Institute of Atmospheric Physics, Chinese Academy of Sciences, No. 40 Building, Bei-Chen-Xi-Lu, Chaoyang District, Beijing 10029, China.
E-mail: drq@mail.iap.ac.cn

DOI: 10.1175/2009MWR2841.1

meridional profile of autocorrelations in the Southern Hemisphere is similar to that in the Northern Hemisphere, but the persistence is less in the Southern Hemisphere. The differences between quasi-stationary forced waves and advection in the two hemispheres possibly play an important role in the persistence differences. Except for the geographical distributions, the intraseasonal and interannual variability of persistence has also been explored. A considerable intraseasonal and interannual variability of persistence of the 500-mb (hPa) height field during the Northern Hemisphere winter was found in the study of Horel (1985a). The persistence of daily 500-mb geopotential height anomalies over the central Pacific as a region with frequent blocking activity is found to change obviously with the sign and magnitude of height anomalies (Horel 1985b).

In recent decades, obvious changes of atmospheric general circulation have been observed (Trenberth and Hurrell 1994; Zhu et al. 2003; Agudelo and Curry 2004; Xiao and Li 2007). The changes of atmospheric general circulation are generally associated with those of the dynamics of atmospheric internal variability, which in turn might change the atmospheric persistence and predictability. Recently, significant decadal changes of persistence and predictability of monthly and seasonal mean circulation have been found in some regions of the tropics and midlatitudes (Goswami 2004; Kang et al. 2006; Ding et al. 2008). It is also possible that there exist considerable decadal variability and trends in the weather persistence. However, up to now, few investigations have been performed investigating the long-term trend and decadal variability of weather persistence. The purpose of this paper is to investigate the trend and decadal variability of persistence of daily geopotential height anomalies for the winter season. The analysis is based on the temporal autocorrelation at every grid point, and the decadal variability of persistence in the Northern Hemisphere (20°–90°N), Southern Hemisphere (20°–90°S), and tropical regions (20°S–20°N) is studied separately. Use of temporal autocorrelation instead of pattern correlation provides us with the results of trend and decadal variability at every grid point, thus allowing us to compare the differences between different regions.

This paper is arranged as follows: The data and analysis method used in this study are described in section 2. Section 3 presents the results and these are discussed in section 4. The conclusions are given in section 5.

2. Data used and methodology

The datasets used in this study include daily geopotential heights and sea level pressure (SLP), monthly air temperature, and zonal winds at 500 mb from the National Centers for Environmental Prediction–National Center for Atmospheric Research (NCEP–NCAR) reanalysis data (1948–2006), the monthly Arctic Oscillation index (AOI; Li and Wang 2003, 1948–2006), the Antarctic Oscillation index (AAOI; Nan and Li 2003, 1948–2006), the Southern Oscillation index (SOI; 1948–2006), and monthly sea surface temperature (SST) from version 2 of the National Oceanic and Atmospheric Administration (NOAA) Extended Reconstructed SST data (1854–2006). Daily 500-mb geopotential heights from the 40-yr European Centre for Medium-Range Weather Forecasts (ECMWF) Re-Analysis (ERA-40) data (1958–2001) are also used to verify results from the NCEP–NCAR reanalysis data. The AOI (AAOI) is defined as the difference in the normalized monthly zonal-mean SLP between 35° and 65°N (40° and 70°S). The period of investigation consists of 58 winter seasons from 1948/49 to 2005/06. Winter is defined as December–January–February and contains 90 days. Following Trenberth (1984), the overall mean and the first four harmonics of the mean annual cycle are used to remove the annual cycle from the daily data, leaving the anomalies. Following Gutzler and Mo (1983), the autocorrelation r_L of a daily time series $x(t)$ of length N days for lag L days is defined as

$$r_L = \frac{\left\{\left[\frac{1}{N}\sum_{i=1}^{N-L} x(i)x(i+L)\right] - \bar{x}^2\right\}}{\sigma^2}, \qquad (1)$$

where

$$\bar{x} = \frac{1}{N}\sum_{i=1}^{N} x(i) \quad \text{and}$$

$$\sigma^2 = \frac{1}{N}\sum_{i=1}^{N} [x(i) - \bar{x}]^2.$$

We compute the autocorrelation of 500-mb height anomalies at each grid point for 58 winter seasons, respectively. Then a 58-yr time series of winter autocorrelations at each grid point is obtained. Based on the 58-yr time series of autocorrelations, the trend and decadal variability of persistence of daily 500-mb geopotential height anomalies can be analyzed. In addition, the trend change of the effective time between independent samples T_0 is also investigated. As in autocorrelation, T_0 is also an important measure of the persistence in the circulation (Madden 1976; Shukla and Gutzler 1983; Trenberth 1985). If all autocorrelations at lag are obtained, then T_0 is given by

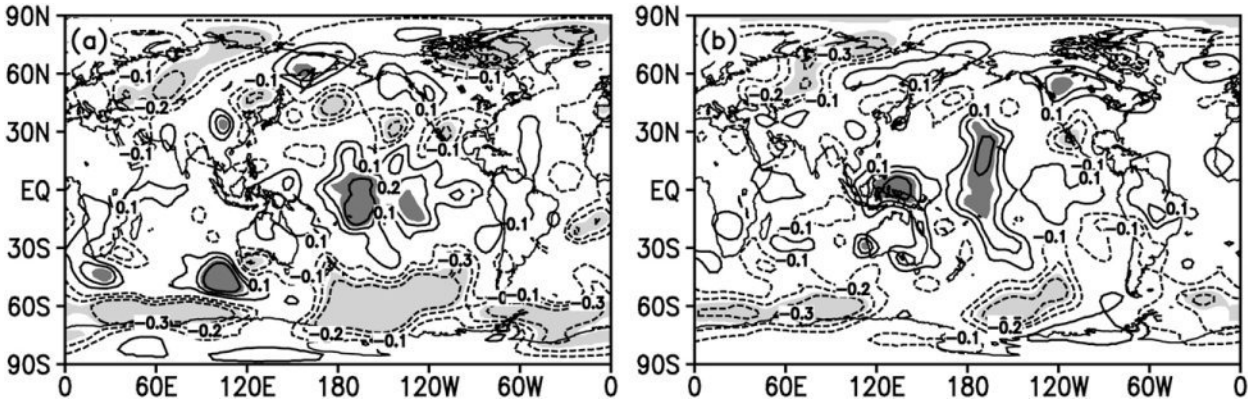

FIG. 1. Linear trend coefficients of winter season autocorrelations at (a) 1- and (b) 5-day lags for the period of 1948–2005. The values in the shaded areas are significant at the 0.05 level.

$$T_0(N) = 1 + 2\sum_{L=1}^{N}\left(1 - \frac{L}{N}\right) r_L, \qquad (2)$$

where T_0 is a function of N and depends on all autocorrelations at lag. Because the r_L at large lags estimated from (1) become unreliable since the number of terms in the summation in (1) diminishes (Jones 1975; Katz 1982), we determine the r_L at large lags following the work of Trenberth (1985). A model autoregressive (AR) process is first fit to the time series. Then the order p of the AR model is identified using the procedure given by Katz (1982). The maximum p considered was limited to 5. After the p model parameters are determined and the first p autocorrelations are computed from the data, other autocorrelations at lags greater than p are computed from the AR model and not from the data. Finally, the T_0 values computed from the autocorrelations utilizing the AR model are used to investigate the long-term trends of the persistence.

3. Results

a. Long-term trends

Figure 1 shows the linear trend coefficients of winter season autocorrelations at 1- and 5-day lags (denoted r_1 and r_5, respectively) of 500-mb height, which show the short- and long-term persistence of daily anomalies, respectively. It is shown that the spatial distribution of linear trend coefficients of r_1 is similar to that of r_5. The parameters r_1 and r_5 both show a significant increasing trend in the tropical Pacific. The parameter r_1, with significant increasing regions mainly in the central and eastern tropical Pacific, is slightly different from r_5, with significant increasing regions mainly in the central and western tropical Pacific. The regions of r_1 and r_5 with significant decreasing trends are mainly located at mid–high latitudes of the Northern and Southern Hemispheres. Over northeast Canada and Greenland, the North Pacific and Northeast China, Northwest Russia, and most regions of southern mid–high latitudes, r_1 shows significant

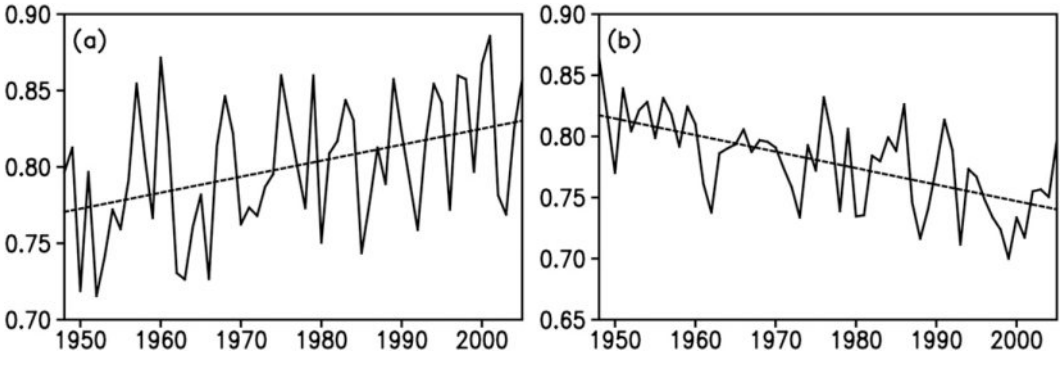

FIG. 2. Area-averaged autocorrelation at 1-day lag for winter in (a) the tropical Pacific region (20°S–5°N, 180°–150°W) and (b) the southern high-latitude region (60°–70°S, 0°–360°). The dashed line indicates the linear trend. The linear trends in (a) and (b) are both significant at the 0.05 level.

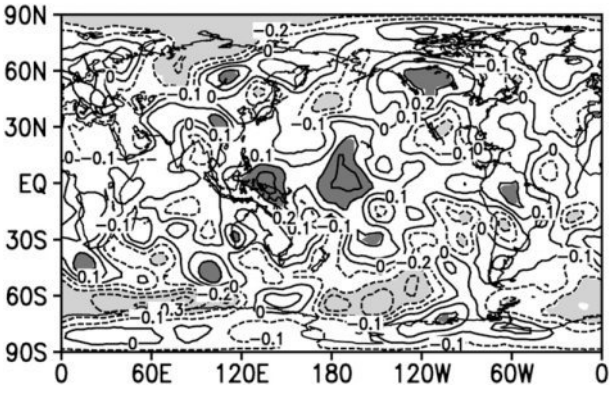

FIG. 3. As in Fig. 1, but for linear trend coefficients of the effective time between independent samples T_0 in winter.

decreasing trends. Compared with r_1, r_5 shows a significant decreasing trend in similar but slightly smaller regions. We choose two regions, the tropical Pacific (20°S–5°N, 180°–150°W) and the southern high latitudes (60°–70°S, 0°–360°), with significant increasing and decreasing trends, respectively, in Fig. 1a. Figure 2 illustrates the variations of area-averaged r_1 in these two regions. It is found that r_1 in the tropical Pacific exhibits not only a remarkable interannual fluctuation, but also a general increasing trend. In the southern high latitudes, r_1 exhibits a relatively weak interannual fluctuation with a decreasing trend. The slope of the linear trend in the tropical Pacific is 0.11 $(100\ \text{yr})^{-1}$ and the variance explained by the linear trend is 19%. The slope of the linear trend in southern high latitudes is $-0.15\ (100\ \text{yr})^{-1}$ and the variance explained by the linear trend is 36%. These linear trends both are significant at the 0.05 level. For these regions, it appears that decadal variations of autocorrelations are dominated by the linear upward or downward trend.

The effective time between independent samples T_0 of 500-mb height for winter shows a significant decreasing trend in the southern mid–high latitudes and the Arctic, while it exhibits a significant increasing trend in the tropical Pacific (Fig. 3). The pattern of trend coefficients of T_0 is similar to that of r_1. Area-averaged T_0 values over the tropical Pacific (10°S–10°N, 180°–150°W) and the southern high latitudes (60°–70°S, 0°–360°) also exhibit remarkable interannual fluctuations superimposed on long-term linear trends (Fig. 4). The slopes of linear trends of T_0 in the tropical Pacific and the southern high latitude are 6 day and -4 day $(100\ \text{yr})^{-1}$, respectively. The variances explained by the linear trends in the tropical Pacific and the southern high latitudes are 18% and 25%, respectively. These linear trends are both significant at the 0.05 level. The T_0 is related to the estimate of climate noise (Trenberth 1984). Thus, the trend changes of T_0 might be associated with the change of potential predictability of climate variability. Further work may be needed to examine whether the potential predictability of climate variability experiences a remarkable change in these regions. If the decay of autocorrelations fits the red noise process, the autocorrelations at lag L can be computed from $r_L = r_1^L$. Therefore, r_5 and T_0 possibly show changes similar to r_1 in those regions where the red noise process occurs. It is indicated that the red noise processes mainly occur in the southern midlatitudes, the equatorial region, the North Pacific, and the North Atlantic for winter (Fig. 5f), consistent with Gutzler and Mo (1983) and Trenberth (1985). Over most of the regions where the red noise process occurs, the order of AR model is relatively stable in different decades and does not experience noticeable change (Figs. 5a–e). This may be the reason why r_1, r_5, and T_0 show similar trends for winter in the southern mid–high latitudes and the tropical Pacific.

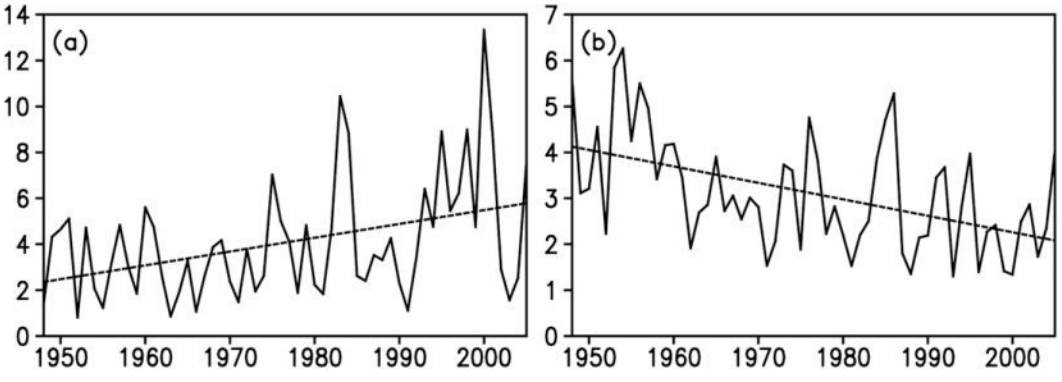

FIG. 4. Area-averaged effective time between independent samples T_0 (in days) over (a) the tropical Pacific region (20°S–5°N, 180°–150°W) and (b) the southern high-latitude region (60°–70°S, 0°–360°). The dashed line indicates the linear trend. The linear trends in (a) and (b) are both significant at the 0.05 level.

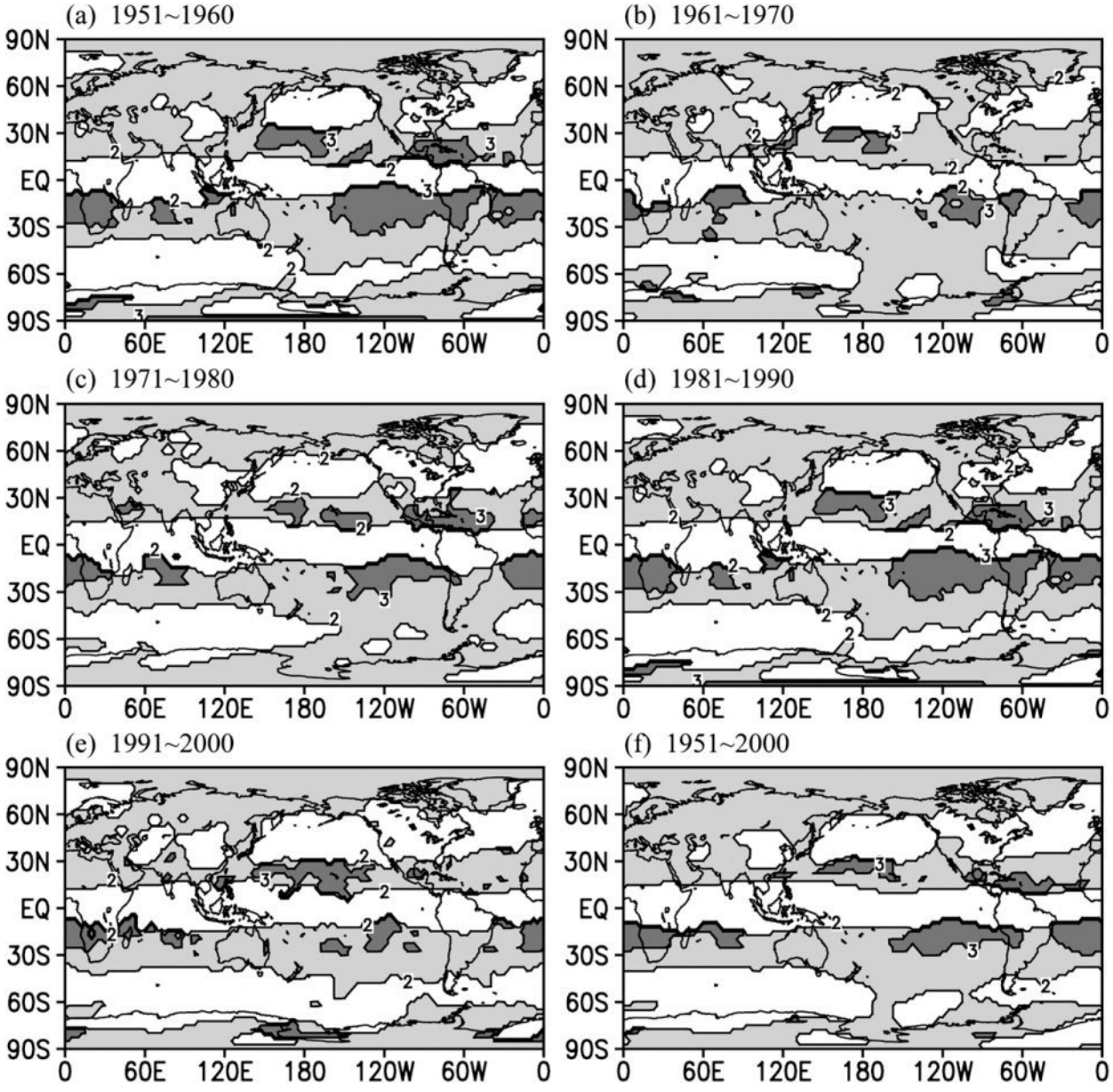

FIG. 5. The order p of AR process fit to the winter 500-hPa height anomalies for (a)–(e) different decades and (f) the whole period. The white regions are where $p = 1$ (red noise).

b. Decadal variability

To emphasize the decadal variability of persistence of daily 500-mb geopotential height anomalies, a 7-yr low-pass Gaussian filter is applied to the time series of winter seasons r_1 and r_5. The linear trend has been removed before the low-pass filtering. The spatial and temporal structures of decadal variability are examined by performing a covariance empirical orthogonal function (EOF) analysis. The EOFs are computed separately for the Northern Hemisphere (20°–90°N), Southern Hemisphere (20°–90°S), and tropics (20°S–20°N). The first EOFs computed on the low-pass-filtered series of winter seasons r_1 and r_5 are shown in Fig. 6. The first EOFs of r_1 and r_5 are denoted as the r_1–EOF1 and r_5–EOF1, respectively. The time series associated with the r_1–EOF1 and r_5–EOF1 are denoted as the r_1–PC1 and r_5–PC1, respectively. For the Northern Hemisphere, the r_1–EOF1 (25.4% explained variance) has the largest anomalies of the same sign occurring off the east coast of Asia and North America and in North Greenland (Fig. 6a). The minima of r_1 during the Northern Hemisphere winter are

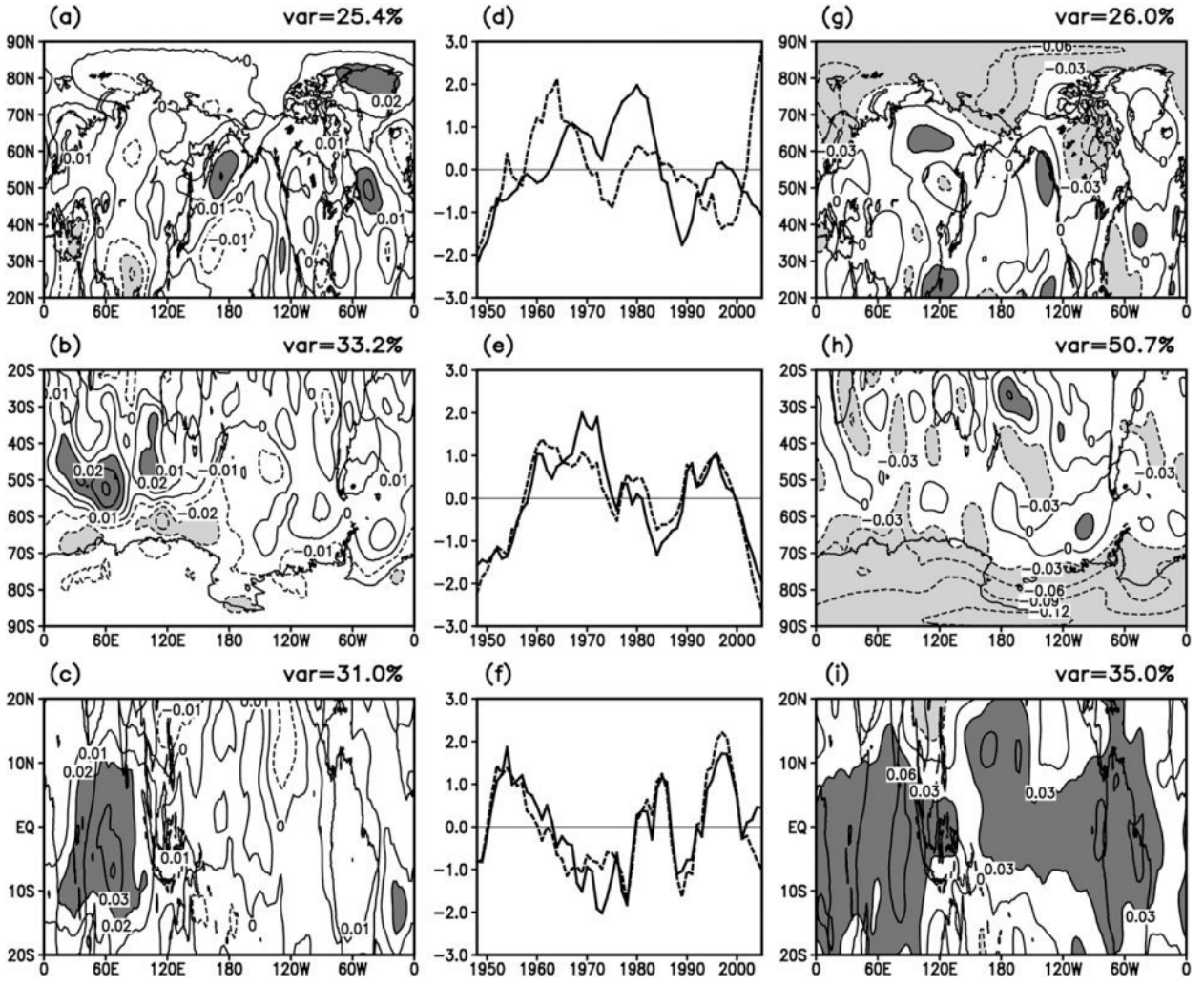

FIG. 6. (left) The first EOF of 7-yr low-pass-filtered series of winter season autocorrelation at 1-day lag in the (a) Northern Hemisphere, (b) Southern Hemisphere, and (c) tropics. (right) The first EOF of winter season autocorrelation at a 5-day lag in the (g) Northern Hemisphere, (h) Southern Hemisphere, and (i) tropics. (d),(e),(f) The time series associated with the first EOFs, with the solid line the time series of the first EOF of autocorrelation at 1-day lag and the dashed line the time series of the first EOF of autocorrelation at 5-day lag. In (a)–(c), the regions with value greater than 0.02 or less than −0.02 are shaded. In (g)–(i), the regions with value greater than 0.03 or less than −0.03 are shaded.

also located off the east coast of Asia and North America, which coincide with the storm track and regions of greatest baroclinicity in the Northern Hemisphere (Klein 1951; Gutzler and Mo 1983). The r_1–EOF1 is possibly related to the decadal variability of the lowest persistence off the east coast of Asia and North America. From the evolution of the r_1–PC1, r_1 is anomalously large off the east coast of Asia and North America from the mid-1960s to the mid-1980s, changing to anomalously small during the late 1980s and early 1990s (Fig. 6d).

When compared with the r_1–EOF1, the magnitude of the r_5–EOF1 (26.0% explained variance) in the Northern Hemisphere is larger, which possibly implies that the decadal variability of long-term persistence is more significant than that of short-term persistence. The r_5–EOF1 is characterized by a prominent negative anomaly in the Arctic (Fig. 6g), with obvious differences with the r_1–EOF1. The time variation of the r_5–EOF1 is also not consistent with that of the r_1–EOF1 (correlation coefficient only 0.23), especially in recent decades when the r_1–PC1 and r_5–PC1 even show an opposite change (Fig. 6d). This is different from the cases of Southern Hemisphere and tropics, where the r_1–EOF1 and r_5–EOF1 show nearly consistent variations (Figs. 6e,f). It is indicated that decadal variability of persistence in the Northern Hemisphere is more complicated and different mechanisms are possibly responsible for the decadal variability of winter season r_1 and r_5.

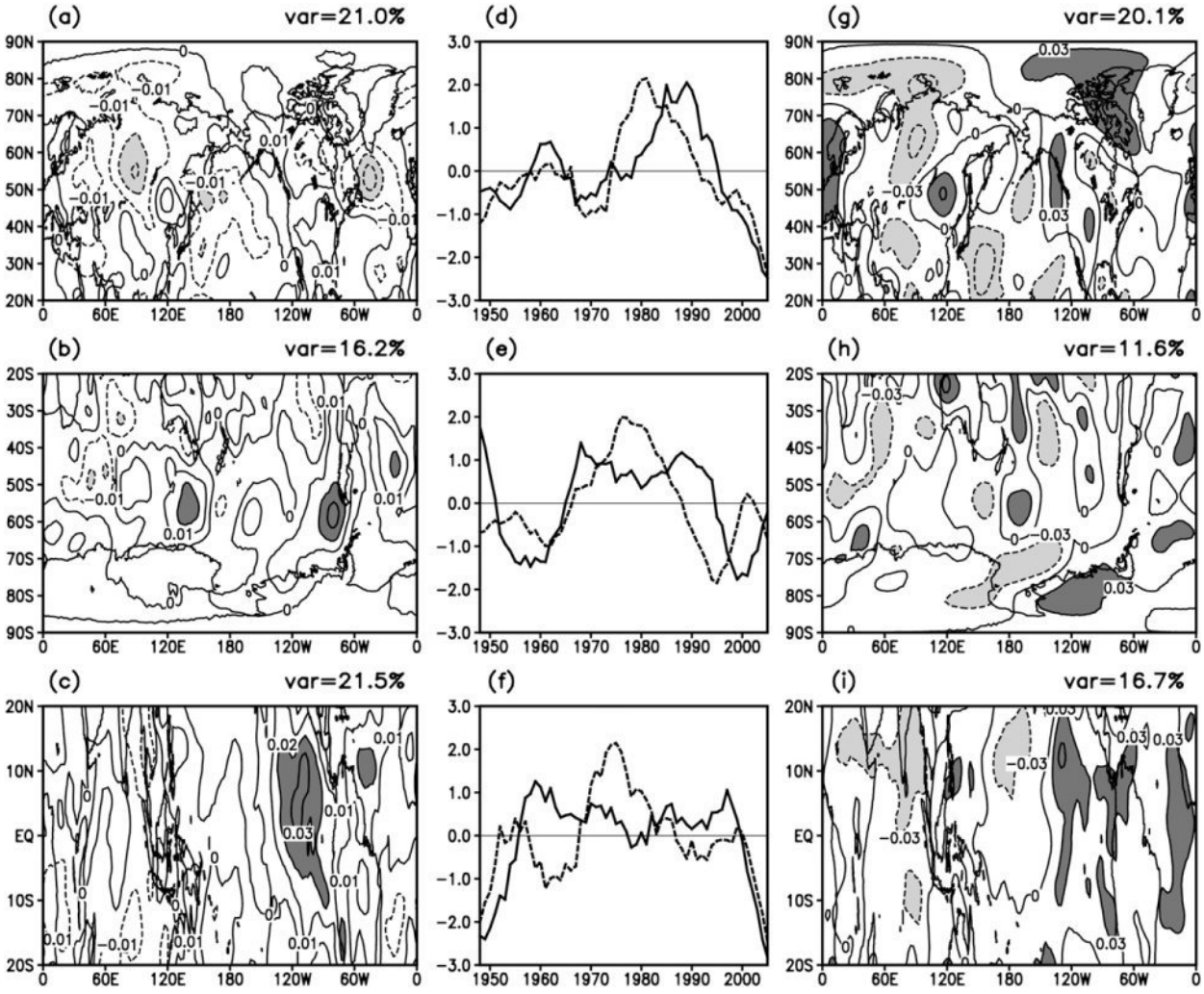

FIG. 7. As in Fig. 6, but for the second EOF of winter season autocorrelations at 1- and 5-day lags.

The r_1–EOF1 in the Southern Hemisphere (33.2% explained variance) has the largest positive amplitude in the midlatitude South Indian Ocean region (Fig. 6b), where the smallest value of r_1 in the climatological mean is found (Trenberth 1985). It seems that the r_1–EOF1 in the Southern Hemisphere is similar to that in the Northern Hemisphere, where the lowest persistence regions show a large anomaly. From the r_5–EOF1 in the Southern Hemisphere, it is obvious that the most prominent negative anomalies are located in the Antarctic (Fig. 6h), which is also similar to the case in the Northern Hemisphere with the most prominent anomalies in Arctic. As mentioned above, the r_1–EOF1 in the Southern Hemisphere show nearly consistent fluctuation with the r_5–EOF1 with correlation coefficient 0.90 (Fig. 6e). The anomalously large values of the r_1–PC1 and r_5–PC1 occur in the 1960s, 1970s, and 1990s.

The r_1–EOF1 in the tropics (31.0% explained variance) shows a large positive anomaly in the tropical Indian Ocean (Fig. 6c). The r_5–EOF1 (35.0% explained variance) shows a more coherent large-scale pattern of positive anomalies than that of r_1 (Fig. 6i). Besides the tropical Indian Ocean, other regions including the tropical Pacific, tropical South America, and tropical Africa have large positive anomalies. It is indicated that the decadal variability of persistence with a longer time lag might correspond to the one with a larger spatial scale. Despite the difference of spatial patterns, the consistency between the r_1–PC1 and r_5–PC1 exists (correlation coefficient 0.88; Fig. 6f). The r_1–PC1 and r_5–PC1 both show the positive phase in the 1950s, mid-1980s, and 1990s, and show the negative phase in the other periods.

Figure 7 gives the second decadal EOFs of winter season r_1 and r_5 (denoted the r_1–EOF2 and r_5–EOF2, respectively) separately in the Northern and Southern

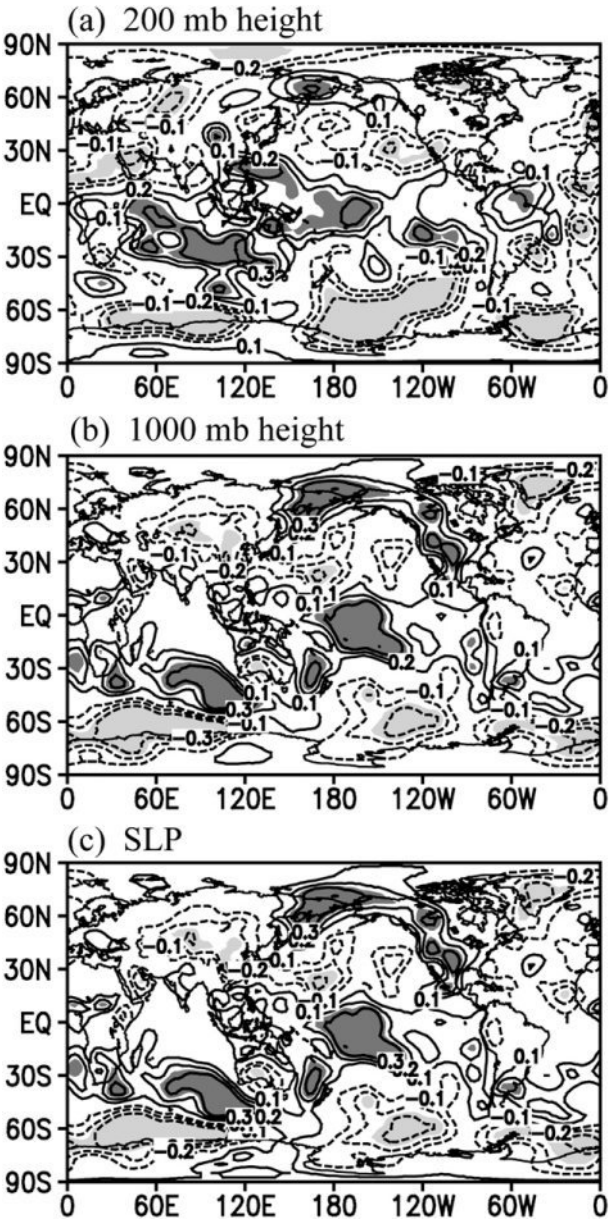

FIG. 8. Linear trend coefficients of autocorrelation at 1 day of (a) 200-mb height, (b) 1000-mb height, and (c) SLP for the period of 1948–2005. The values in the shaded areas are significant at the 0.05 level.

Hemispheres and tropics. In comparison with the first EOFs, the r_1–EOF2 and r_5–EOF2 have more complicated spatial patterns, which seems to be related to local spatial structures of decadal variability of winter season r_1 and r_5. It is very difficult for us to explain what phenomena correspond to the spatial patterns of the second EOFs. However, in view of the relatively high explained variance of the r_1–EOF2 and r_5–EOF2 (explained variance presented in Fig. 7), it is very important to further explore implication of the second EOFs in the future work. From the time series associated with the r_1–EOF2 and r_5–EOF2 (denoted the r_1–PC2 and r_5–PC2, respectively), the r_1–PC2 shows nearly consistent fluctuation with the r_5–PC2 in the Northern Hemisphere (correlation coefficient 0.72), while the r_1–PC2 has relatively low correlation with the r_5–PC2 in the Southern Hemisphere and tropics (correlation coefficients 0.40 and 0.47, respectively).

4. Discussion

Besides the 500-mb height anomalies, the linear trends of winter season r_1 of 200-mb height, 1000-mb height, and SLP anomalies are also investigated. For these variables, it is found from Fig. 8 that the spatial distribution of linear trend coefficients of r_1 is very similar to that of 500-mb height. The parameter r_1 also exhibits significant increasing trends in most regions of the tropical Pacific, and shows significant decreasing trends in most regions of the southern mid–high latitudes (Fig. 8). In addition, the persistence of these variables also shows significant decadal variability similar to that of 500-mb height (not shown). The results suggest that there are prominent trends and decadal variability of persistence of daily anomalies of atmospheric circulation in some regions of the world. A question of great interest is the origin of trends and decadal variability of persistence. In the southern mid–high latitudes, Trenberth (1985) showed that the baroclinicity and advection are two important factors affecting the persistence. The baroclinicity itself can cause strong development of new disturbances. Even in the absence of disturbance development, the strong advection in the westerlies moves a disturbance quickly across a given location, thereby reducing the autocorrelations. We examine the changes of the baroclinicity and advection in the southern mid–high latitudes. The baroclinicity is measured by the meridional temperature gradient in the troposphere. Figure 9a shows the difference of 500-mb zonal-mean temperature between 50° and 70°S. It is indicated that the winter meridional temperature gradient between 50° and 70°S increases continuously since the 1950s. As a result of larger meridional temperature gradient, the baroclinicity between 50° and 70°S also increases. Thus, atmospheric persistence will get lower in the regions between 50° and 70°S. The correlation coefficient between the temperature difference in Fig. 9a and the area-averaged r_1 over the southern mid–high latitudes in Fig. 2b is -0.75, which is significant at the 0.05 level. It is implied that the significant downward trend of the persistence occurring in the southern mid–high latitudes is closely associated with the increase of meridional

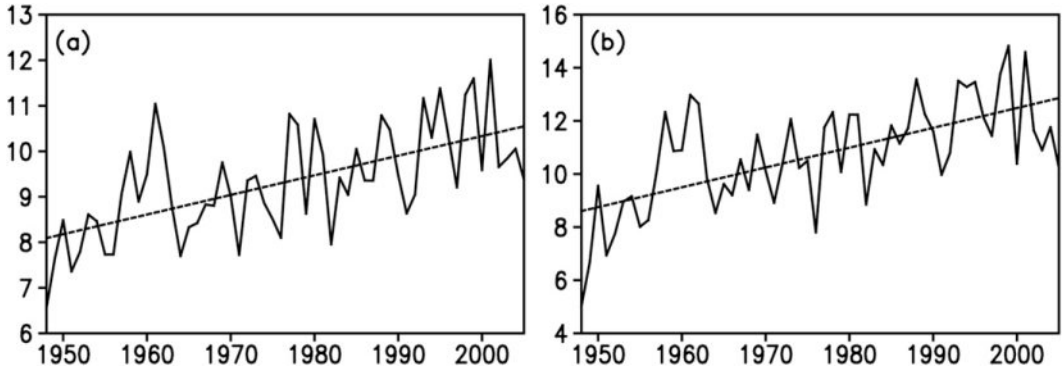

FIG. 9. Time series of the (a) difference in the 500-mb zonal-mean temperature (°C) between 50° and 70°S and (b) the area-averaged 500-mb zonal wind (m s^{-1}) over the southern midlatitudes (50°–70°S, 0°–360°) during winter.

temperature gradient there. The increase of meridional temperature gradient between 50° and 70°S is found to be related to global climate change. After the late 1970s, the winter temperature at 500 mb in the southern midlatitudes significantly increases, while that in Antarctic significantly decreases (Fig. 10), thus causing the meridional temperature gradient between 50° and 70°S to increase. In addition, the enhanced meridional temperature gradient is associated with the increase of zonal winds between 50° and 70°S (Fig. 9b). The stronger zonal wind, corresponding to a stronger advection, may account for the generally lower levels of persistence. The correlation coefficient between the area-averaged zonal winds over the southern mid–high latitudes in Fig. 9b and the area-averaged r_1 over the southern mid–high latitudes in Fig. 2b is −0.79, which is significant at the 0.05 level. Therefore, the enhanced baroclinicity and the associated enhanced advection appear to be responsible for the decrease in the persistence of daily anomalies of atmospheric circulation in the southern mid–high latitudes since the 1950s. Together with the increase in the meridional temperature gradient between 50° and 70°S, there is a corresponding decrease in the meridional temperature gradient between 30° and 50°S (Fig. 10). However, there is no significant increasing trend in the persistence in the most regions between 30° and 50°S for either r_1 or r_5 (Fig. 1). The reason for this phenomenon remains unexplained. In the ERA-40 reanalysis, the r_1 shows significant increasing trend in a wide region between 30° and 50°S (Fig. 15). It is speculated that the biases of the climate trends in the NCEP–NCAR reanalysis data possibly lead to the inconsistency of the trend of persistence. This question is left for further study. From Fig. 10, it is also noted that the temperature gradient in the Asia–European continent, North Pacific, and North Atlantic increases in recent decades, which corresponds well with the downward trend of r_1 in these regions (Fig. 1a).

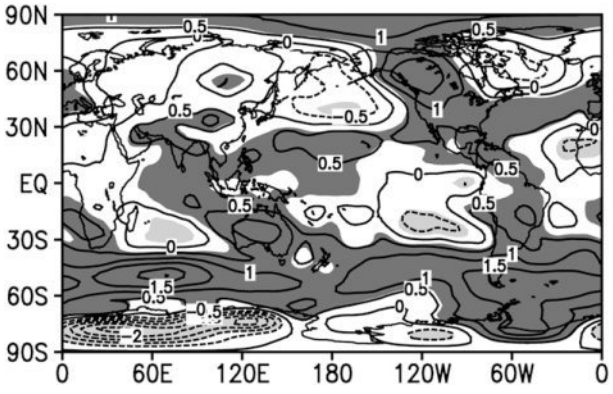

FIG. 10. Composite difference of winter temperature at 500 mb (°C) between 1979–2005 and 1948–78. The values in the shaded areas are significant at the 0.05 level of the *t* test.

Different from the southern mid–high latitudes, there might be other mechanisms responsible for the upward trend of persistence in the tropical Pacific. Trenberth (1985) showed that the high persistence of daily geopotential heights in the tropics is linked to the low-frequency coupling between the atmospheric circulation and SST. Figure 11 shows that the inverse relationship between the winter Niño-3 (5°S–5°N, 150°–90°W) SSTA and SOI has enhanced from the 1980s to the 1990s. It is indicated that the coupling between the SST and atmospheric circulation in the tropical Pacific becomes stronger from the 1980s to the 1990s, which could contribute to the longer persistence in the tropical Pacific in this period. Figure 12 shows that tropical Pacific SST variability significantly increases in recent decades, consistent with Knutson et al. (1997) and Gu and Philander (1997). The increased SST variability could exert a stronger external forcing on the tropical Pacific atmosphere that tends to enhance the coupling between the

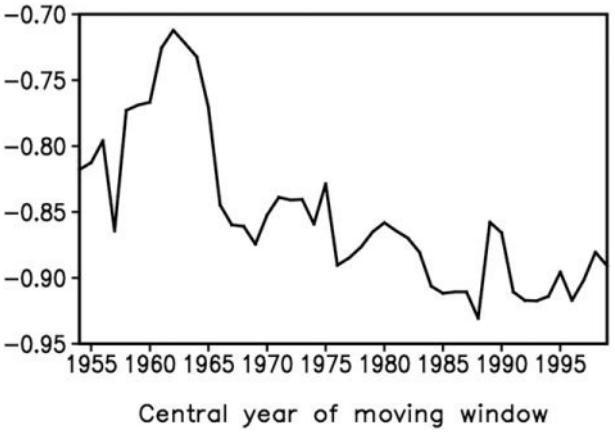

FIG. 11. The 13-yr sliding correlations between the winter SOI and the winter Niño-3 (5°S–5°N, 150°–90°W) SSTA during 1948–2005. All correlations are significant at the 0.05 level.

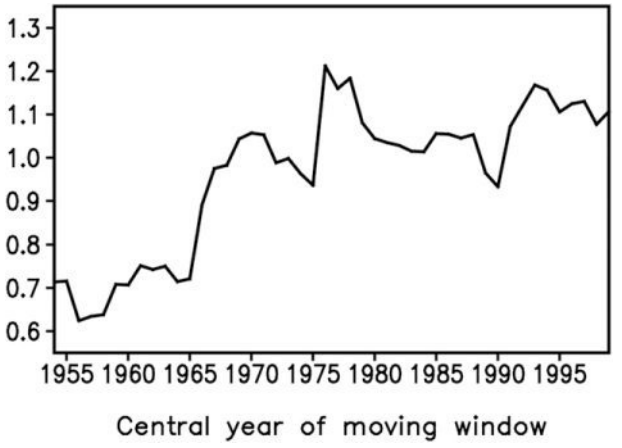

FIG. 12. Time series of running standard deviation of winter Niño-3 (5°S–5°N, 150°–90°W) SSTA (°C) calculated within a 13-yr window that moves year by year from 1948 to 2005.

SST and atmospheric circulation in the tropical Pacific. This process is favorable to the increase of atmospheric persistence in the tropical Pacific in recent decades. However, the shapes of curves shown in Figs. 2a and 4a are very different from those in Figs. 11 or 12, although their trends are similar. It is indicated that other important reasons responsible for the increase of atmospheric persistence in the tropical Pacific might not be touched. We will continue to examine the results in the future and try to find possible reasons.

The mechanism driving the decadal variability of the persistence of daily 500-mb geopotential height anomalies remains unexplained, but we note that there is some linkage between decadal variability of the persistence and large-scale atmospheric circulation patterns. The Arctic Oscillation (AO) and the Antarctic Oscillation (AAO) are major modes of low-frequency variability in the Northern and Southern Hemispheres, respectively (Thompson and Wallace 1998; Li and Wang 2003). Figure 13 compares the decadal fluctuations of winter AOI (AAOI) with the r_5–PC1 in the Northern Hemisphere (Southern Hemisphere). A good relationship is found between them and correlation coefficients are −0.75 and 0.71 (both significant at the 0.05 level) for the Northern Hemisphere and Southern Hemisphere, respectively. In comparison with the r_5–PC1, the relationships of the r_1–PC1 in the Northern Hemisphere (Southern Hemisphere) with winter AOI (AAOI) are similar, with the correlation coefficients −0.68 and 0.70, respectively. One possible reason for this good relationship is that the AO and AAO involve a zonally symmetric climate seesaw between the high latitudes and the midlatitudes in the Northern and Southern Hemispheres. The decadal variations of the AOI and

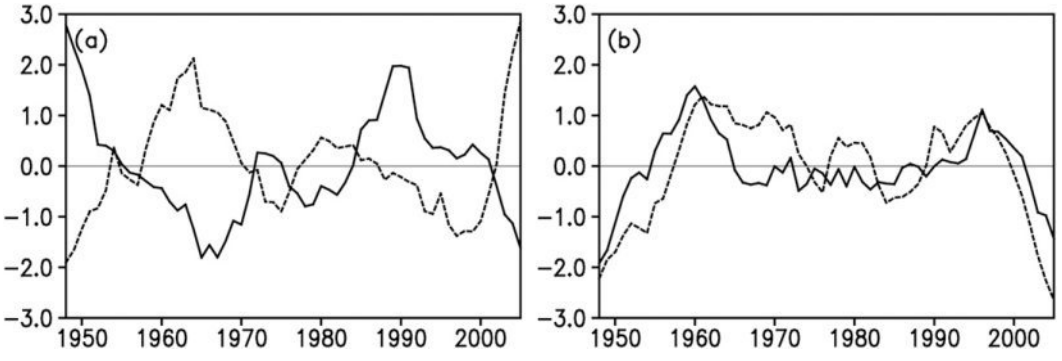

FIG. 13. (a) Time series of 7-yr low-pass-filtered winter AOI (solid line) and the time series associated with the first EOF of winter season autocorrelation at the 5-day lag in the Northern Hemisphere shown in Fig. 6d (dashed line). (b) Time series of 7-yr low-pass-filtered winter AAOI (solid line) and the time series associated with the first EOF of winter season autocorrelation at the 5-day lag in the Southern Hemisphere shown in Fig. 6e (dashed line). The linear trends of AOI and AAOI have been removed before the low-pass filter.

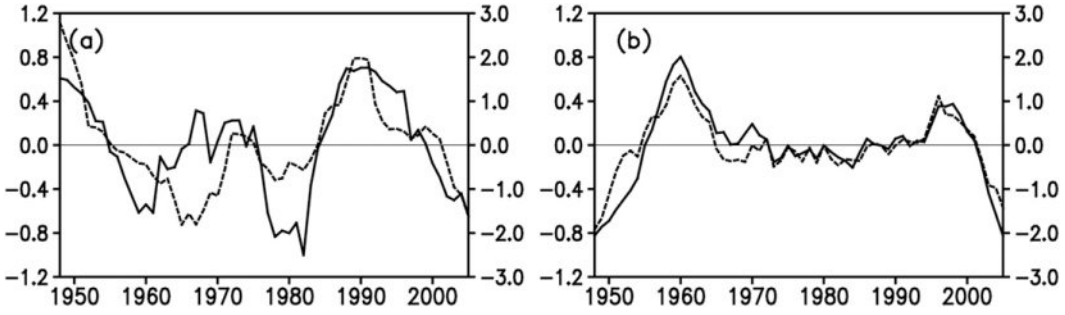

FIG. 14. (a) The 7-yr low-pass-filtered time series of winter 500-mb temperature difference (°C) between 40° and 60°N (solid line) and winter AOI (dashed line). (b) The 7-yr low-pass-filtered time series of winter 500-mb temperature difference (°C) between 40° and 70°S and winter AAOI (dashed line).

AAOI are well related to those of the meridional temperature gradient between the midlatitudes and the high latitudes in the Northern and Southern Hemispheres, respectively (Fig. 14). The correlation coefficient between the decadal variability of winter AOI (AAOI) and the meridional temperature gradient between the midlatitudes and the high latitudes in the Northern Hemispheres in Fig. 14a (the Southern Hemispheres in Fig. 14b) is 0.91 (0.86) (both significant at the 0.05 level), respectively. As mentioned above, the baroclinicity due to the meridional temperature gradient between the midlatitudes and the high latitudes is an important factor affecting the persistence in the midhigh latitudes. The decadal variability of the AO and the AAO is associated with decadal fluctuations of the baroclinicity in the mid–high latitudes in the Northern and Southern Hemispheres, which in turn contribute to the decadal variability of persistence of daily anomalies of atmospheric circulation. Another possible reason for good relationship between the AO (AAO) and the persistence is that decadal variations of the AO (AAO) are closely associated with those of stationary planetary waves. Limpasuvan and Hartmann (1999) showed that variations of the AO are forced by eddy fluxes mainly of stationary waves in the troposphere of the Northern Hemisphere. The interannual and decadal variations of stationary planetary waves in the Northern Hemisphere winter are both closely related to the AO (Chen et al. 2003; Chen 2006). Because the changes in the stationary planetary waves have an important influence on the persistence (Trenberth 1980, 1985), decadal variations of the AO (AAO), associated with the changes of stationary planetary waves in the Northern Hemisphere (Southern Hemisphere), can be linked to decadal variability of the persistence. In addition, Cai et al. (2005) showed that the oceanic overturning circulation anomalies associated with the AAO contribute to the maintenance of the meridional temperature gradient in the southern mid–high latitudes. Therefore, it is also possible that the oceanic overturning circulation associated with the AO and AAO contribute to the decadal variability of long-term persistence of daily anomalies of atmospheric circulation. However, these are only preliminary analysis on the causes of decadal variability of

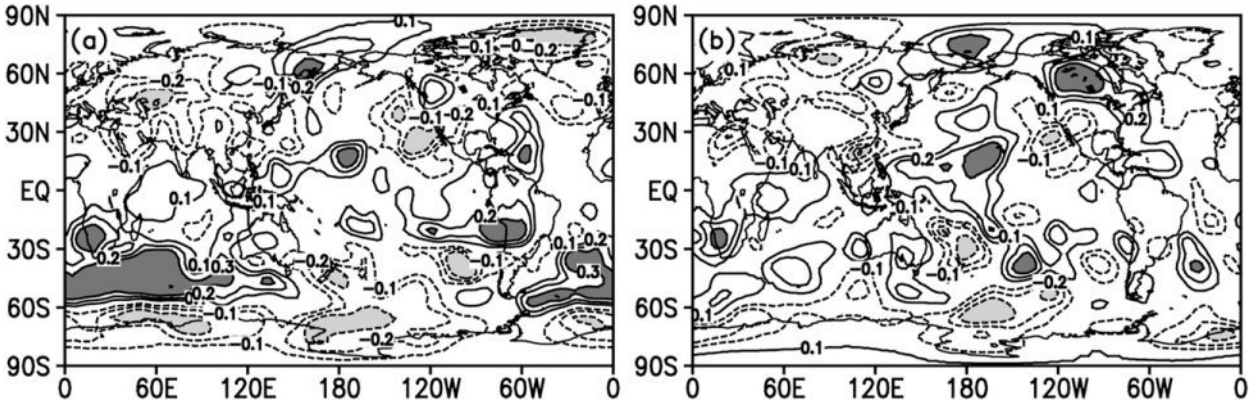

FIG. 15. As in Fig. 1, but for the linear trend coefficients of winter season autocorrelations of daily 500-mb geopotential height anomalies from the ERA-40 reanalysis data (1958–2001).

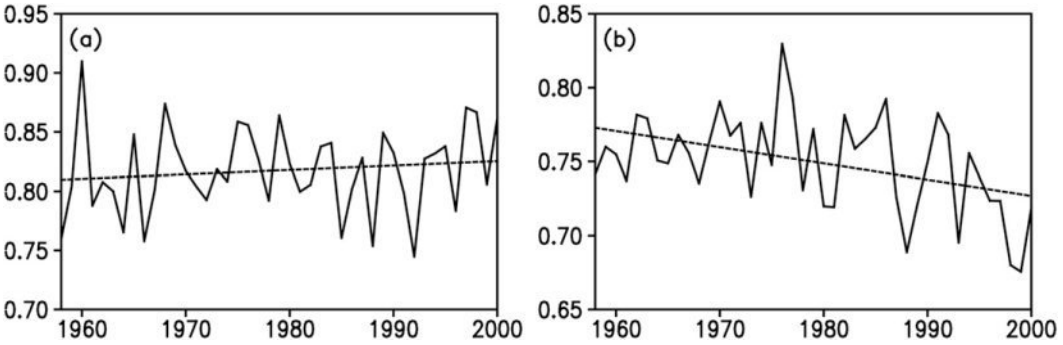

FIG. 16. As in Fig. 2, but for area-averaged autocorrelation at the 1-day lag of daily 500-mb geopotential height anomalies from the ERA-40 reanalysis data (1958–2001).

the persistence. It is necessary to examine the relevant mechanisms using a global atmospheric circulation model in the future.

Another question of great interest is the implications of long-term trend of persistence for weather forecasting. It is shown that as a result of the developments of the observation system and data assimilation technique, the skill of global numerical weather forecasting has been significantly improved in the past 30 yr (Kalnay 2003). However, considering the fact that forecasts are less accurate when persistence is low, the decreased persistence in the mid–high latitudes of the Northern and Southern Hemispheres could have a negative influence on the skill of weather forecasting there, which conflicts with the significant improvement of numerical weather forecasting skill in the past 30 yr. A possible explanation is that the better numerical techniques and the increases in our understanding of the relevant physics (parameterizations) have been a key component in improving weather forecasts over the last few decades. The improvements of numerical techniques and parameterizations might mask the decreasing persistence.

There are two caveats to this study. First, while the NCEP–NCAR reanalysis is one of the most used datasets in the climate community and constitutes the main database for this study, some cautions should be given when considering the atmospheric decadal changes. Some spurious decadal changes due to the observational discontinuities have been found in the NCEP–NCAR reanalysis data (Kistler et al. 2001; Inoue and Matsumoto 2004). Especially for the oceanic areas in the tropics and the Southern Hemisphere, which are exactly the regions where significant trends of the persistence are found in this study, the NCEP–NCAR reanalysis data contains biases in the climate trends (Hines et al. 2000; Marshall 2002, 2003). To justify the results obtained from the NCEP–NCAR reanalysis data, Fig. 15 shows the linear trend coefficients of winter season autocorrelations of daily 500-mb geopotential height anomalies from the ERA-40 reanalysis data. It is found from Fig. 15 that some regions in the southern high latitudes (50°–70°S) exhibit a significant decreasing trend, while most regions in the tropical Pacific show an increasing trend. These results are similar to those from the NCEP–NCAR data (Fig. 1), indicating that the trends of the persistence in these regions may be not entirely spurious in the NCEP–NCAR data. However, there also exist some differences between the NCEP–NCAR and ERA-40 reanalysis data. The regions in the southern high latitudes with a significant decreasing trend from the NCEP–NCAR data are larger than those from the ERA-40 data. On the contrary, a larger region in the southern midlatitudes (30°–50°S) shows a significant increasing trend in the ERA-40 reanalysis than in the NCEP–NCAR reanalysis. The area averages r_1 in the southern high latitude (60°–70°S, 0°–360°) exhibits a little weaker downward trend in the ERA-40 data, with the slope of the linear trend is $-0.11\ (100\ \text{yr})^{-1}$ (Fig. 16b). The slope of the linear trend of the area average of r_1 in the tropical Pacific (20°S–5°N, 180°–150°W) is only $0.04\ (100\ \text{yr})^{-1}$ in the ERA-40 data (Fig. 16a), significantly lower than that in the NCEP–NCAR data (Fig. 2a). Besides, by projecting the time series associated with the first EOFs shown in Fig. 6 on the ERA-40 data (1958–2001), it is found that spatial patterns of decadal variability of persistence in the ERA-40 data are different from those in the NCEP–NCAR data. Especially for the r_5 in the Northern Hemisphere, the r_1 in the Southern Hemisphere and tropics, decadal variability of persistence in the ERA-40 data is not significant with very small anomalies (Fig. 17). Similarly, by projecting the time series associated with the second EOFs shown in Fig. 7 on the ERA-40 data, we found that some differences also exist in the second principal spatial modes from the NCEP–NCAR and ERA-40 reanalysis data (Fig. 18).

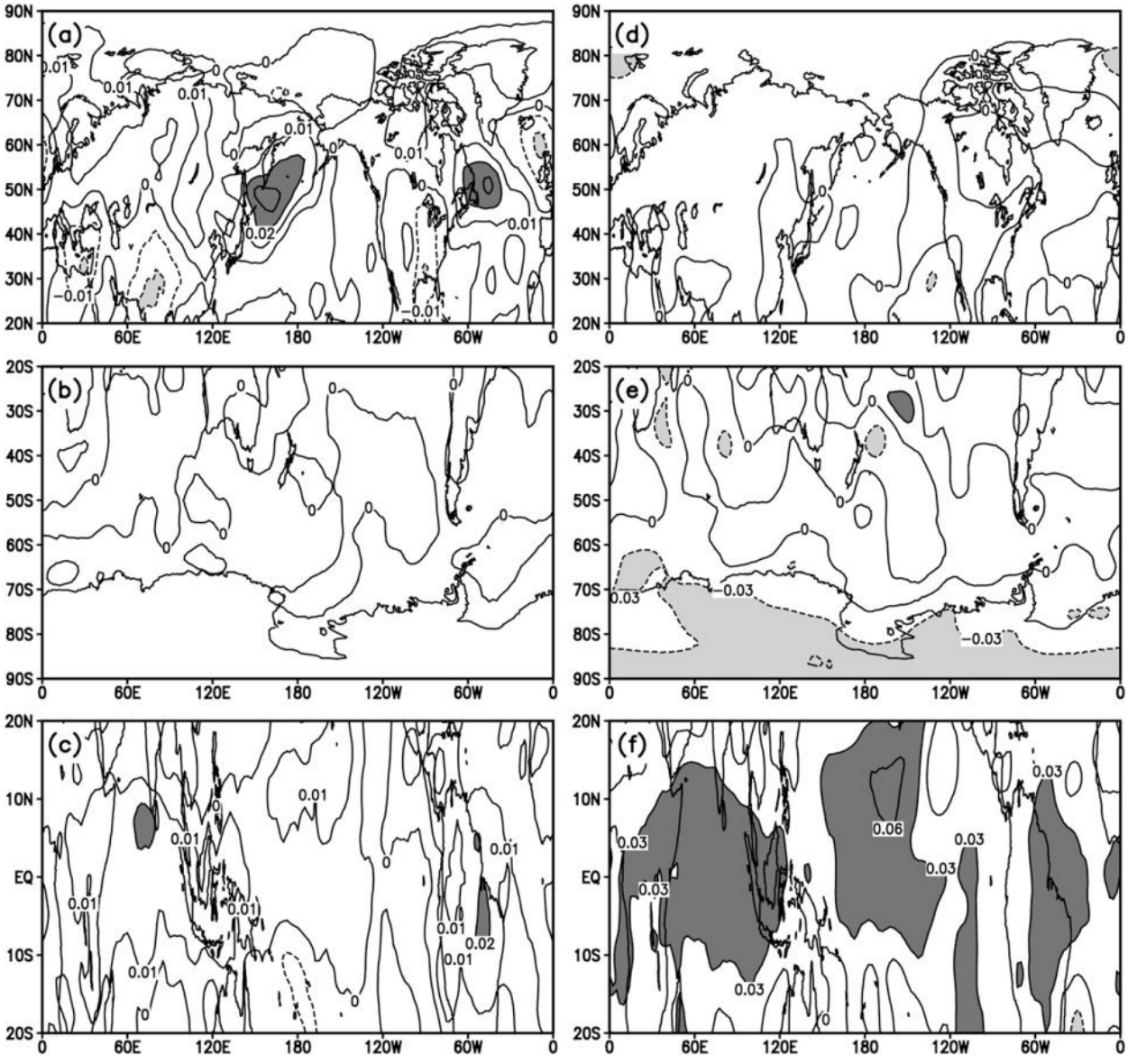

FIG. 17. Spatial patterns obtained by projecting the time series (1958–2001) associated with the first EOFs shown in Fig. 6 on the ERA-40 reanalysis data. (left) The projected spatial patterns of winter season autocorrelation at the 1-day lag in the (a) Northern Hemisphere, (b) Southern Hemisphere, and (c) tropics. (right) The projected spatial patterns of winter season autocorrelation at the 5-day lag in the (d) Northern Hemisphere, (e) Southern Hemisphere, and (f) tropics. In (a)–(c), the regions with values greater than 0.02 or less than −0.02 are shaded. In (d)–(f), the regions with values greater than 0.03 or less than −0.03 are shaded.

The differences between the two reanalysis data leave some uncertainties about whether the linear trends and decadal variability of persistence obtained from the NCEP–NCAR reanalysis are spurious in some regions. Further work should be performed to compare the results of decadal changes of atmospheric persistence with other observational data. Second, when examining the decadal variability of the persistence, a 7-yr low-pass Gaussian filter is applied to the time series of winter season r_1 and r_5 in this study. The 7-yr low-pass filter makes the effective degree of freedom of 58-yr time series very small (at most 8 at each point). For so small a degree of freedom, the EOFs with relatively low explained variance might not be statistically meaningful and may be due to the random noise. For different regions, decadal variability of the persistence might be significantly different. Thus, it is very difficult to extract a dominant pattern of decadal variability of the persistence. The comparisons of decadal variability of the persistence in different regions are left for further study.

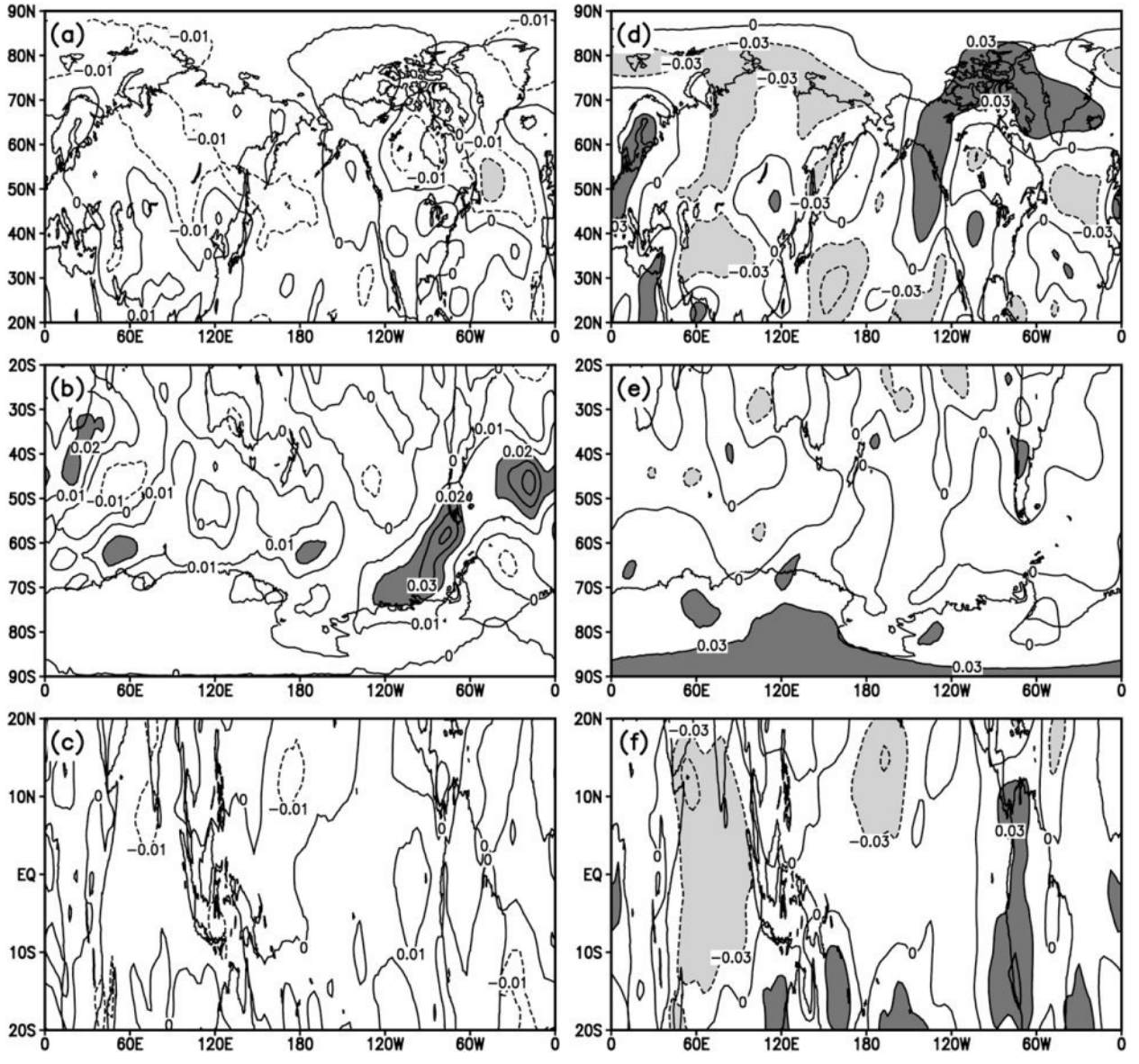

FIG. 18. As in Fig. 17, but for spatial patterns obtained by projecting the time series (1958–2001) associated with the second EOFs shown in Fig. 7 on the ERA-40 reanalysis data.

5. Conclusions

In this paper we investigate the trend and decadal variability of persistence of daily 500-mb geopotential height anomalies for winter season. The persistence is measured based on autocorrelations at 1- and 5-day lags (denoted r_1 and r_5, respectively) and the effective time between independent samples T_0. The results from linear trend analysis show that there exist significant trends of persistence of daily 500-mb geopotential height anomalies in some regions of the world. The regions with significant decreasing trend are found to be mainly located at mid–high latitudes of the Northern and Southern Hemispheres, which include northeast Canada, the North Pacific, northwest Russia, and the southern high latitudes. The regions with significant increasing trend are mainly located in the tropical Pacific. It is speculated that the enhanced baroclinicity and advection are possibly responsible for the significant downward trend of persistence mainly occurring in the southern and northern mid–high latitudes, while the increased coupling between the atmospheric circulation and SST could contribute to the increase of persistence in the tropical Pacific.

An EOF analysis is applied to the low-pass-filtered series of r_1 and r_5 after the linear trend is removed. The EOF analysis shows that there is prominent decadal variability of persistence in some regions of the Northern and Southern Hemispheres and tropics. For the first EOF of r_1, the regions with prominent decadal variability are mainly located off the east coast of Asia and North America, in the midlatitude South Indian Ocean region, and in the tropical Indian Ocean. Instead, r_5 shows prominent decadal variability mainly in the Arctic, the Antarctic, and the tropical Indian Ocean and Pacific. In comparison with r_1, r_5 has decadal variations with larger magnitude and larger spatial scale. Although the spatial patterns of the EOFs of r_1 are totally different from those of r_5, the time series associated with the EOFs of r_1 and r_5 sometimes show nearly consistent variations. In this case the decadal variability of r_1 and r_5 is possibly due to the same mechanisms. Decadal variability of persistence is found to be closely related to decadal fluctuations of large-scale atmospheric circulation patterns. However, further study is necessary to examine how decadal fluctuations of atmospheric circulation influence the decadal variability of persistence.

Acknowledgments. We thank the anonymous reviewers for their helpful comments and suggestions. We thank Prof. M. Mu for many useful comments and for his help with mathematics. Funding for this research was provided jointly by the 973 Program (2006CB403600) and NSFC Projects (40805022 and 40675046).

REFERENCES

Agudelo, P. A., and J. A. Curry, 2004: Analysis of spatial distribution in tropospheric temperature trends. *Geophys. Res. Lett.,* **31,** L222207, doi:10.1029/2004GL020818.

Cai, W., G. Shi, and Y. Li, 2005: Multidecadal fluctuations of winter rainfall over south Western Australia simulated in the CSIRO Mark 3 coupled model. *Geophys. Res. Lett.,* **32,** L12701, doi:10.1029/2005GL022712.

Chen, W., 2006: Decadal variations of quasi-stationary planetary wave propagation in the northern hemisphere winter. *Prog. Nat. Sci.,* **16,** 101–105.

——, M. Takahashi, and H. F. Graf, 2003: Interannual variations of stationary planetary wave activity in the northern winter troposphere and stratosphere and their relations to NAM and SST. *J. Geophys. Res.,* **108,** 4797, doi:10.1029/2003JD003834.

Ding, R. Q., J. P. Li, and K.-J. Ha, 2008: Decadal change of January and July persistence of monthly mean 500 mb geopotential height anomalies. *Geophys. Res. Lett.,* **35,** L02703, doi:10.1029/2008GL034137.

Goswami, B. N., 2004: Interdecadal change in potential predictability of the Indian summer monsoon. *Geophys. Res. Lett.,* **31,** L16208, doi:10.1029/2004GL020337.

Gu, D., and S. G. H. Philander, 1997: Interdecadal climate fluctuations that depend on exchanges between the tropics and extratropics. *Science,* **275,** 805–807.

Gutzler, D. S., and K. C. Mo, 1983: Autocorrelation of Northern Hemisphere geopotential heights. *Mon. Wea. Rev.,* **111,** 155–164.

Hines, K. M., D. H. Bromwich, and G. J. Marshall, 2000: Artificial surface pressure trends in the NCEP–NCAR reanalysis over the Southern Ocean and Antarctica. *J. Climate,* **13,** 3940–3952.

Horel, J. D., 1985a: Persistence of the 500 mb height field during Northern Hemisphere winter. *Mon. Wea. Rev.,* **113,** 2030–2042.

——, 1985b: Persistence of wintertime 500 mb height anomalies over the central Pacific. *Mon. Wea. Rev.,* **113,** 2043–2048.

Inoue, T., and J. Matsumoto, 2004: A comparison of summer sea level pressure over east Eurasia between NCEP-NCAR reanalysis and ERA-40 for the period 1960-99. *J. Meteor. Soc. Japan,* **82,** 951–958.

Jones, R. H., 1975: Estimating the variance of time averages. *J. Appl. Meteor.,* **14,** 159–163.

Kalnay, E., 2003: *Atmospheric Modeling, Data Assimilation and Predictability*. Cambridge University Press, 364 pp.

Kang, I. S., E. K. Jin, and K. H. An, 2006: Secular increase of seasonal predictability for the 20th century. *Geophys. Res. Lett.,* **33,** L02703, doi:10.1029/2005GL024499.

Katz, R. W., 1982: Statistical evaluation of climate experiments with general circulation models: A parametric time series modeling approach. *J. Atmos. Sci.,* **39,** 1446–1455.

Kistler, R., and Coauthors, 2001: The NCEP–NCAR 50-Year Reanalysis: Monthly means CD-ROM and documentation. *Bull. Amer. Meteor. Soc.,* **82,** 247–267.

Klein, W. H., 1951: A hemispheric study of daily pressure variability at sea level and aloft. *J. Meteor.,* **8,** 332–346.

Knutson, T. R., S. Manabe, and D. Gu, 1997: Simulated ENSO in a global coupled ocean–atmosphere model: Multidecadal amplitude modulation and CO_2 sensitivity. *J. Climate,* **10,** 138–161.

Li, J. P., and J. X. L. Wang, 2003: A modified zonal index and its physical sense. *Geophys. Res. Lett.,* **30,** 1632, doi:10.1029/2003GL017441.

Limpasuvan, V., and D. L. Hartmann, 1999: Eddies and the annular modes of climate variability. *Geophys. Res. Lett.,* **26,** 3133–3136.

Macdonald, N. J., and R. Shapiro, 1964: A relationship between persistence and numerical weather prediction. *J. Appl. Meteor.,* **3,** 336–337.

Madden, R. A., 1976: Estimates of the natural variability of time-averaged sea level pressure. *Mon. Wea. Rev.,* **104,** 942–952.

Marshall, G. J., 2002: Trends in Antarctic geopotential height and temperature: A comparison between radiosonde and NCEP–NCAR reanalysis data. *J. Climate,* **15,** 659–674.

——, 2003: Trends in the southern annular mode from observations and reanalyses. *J. Climate,* **16,** 4134–4143.

Nan, S. L., and J. P. Li, 2003: The relationship between the summer precipitation in the Yangtze River valley and the boreal spring Southern Hemisphere annular mode. *Geophys. Res. Lett.,* **30,** 2266, doi:10.1029/2003GL018381.

Shukla, J., and D. Gutzler, 1983: Interannual variability and predictability of 500 mb geopotential heights over the Northern Hemisphere. *Mon. Wea. Rev.,* **111,** 1273–1279.

Thompson, D. W. J., and J. M. Wallace, 1998: The Arctic Oscillation signature in the wintertime geopotential height and temperature fields. *Geophys. Res. Lett.,* **25,** 1297–1300.

Tracton, M. S., K. Mo, W. Chen, E. Kalnay, R. Kistler, and G. White, 1989: Dynamical extended range forecasting (DERF) at the

National Meteorological Center. *Mon. Wea. Rev.,* **117,** 1604–1635.

Trenberth, K. E., 1980: Planetary waves at 500 mb in the Southern Hemisphere. *Mon. Wea. Rev.,* **108,** 1378–1389.

——, 1984: Some effects of finite sample size and persistence on meteorological statistics. Part II: Potential predictability. *Mon. Wea. Rev.,* **112,** 2369–2379.

——, 1985: Persistence of daily geopotential heights over the Southern Hemisphere. *Mon. Wea. Rev.,* **113,** 38–53.

——, and J. W. Hurrell, 1994: Decadal atmospheric-ocean variations in the Pacific. *Climate Dyn.,* **9,** 303–309.

Xiao, D., and J. P. Li, 2007: Spatial and temporal characteristics of the decadal abrupt changes of global atmosphere-ocean system in the 1970s. *J. Geophys. Res.,* **112,** D24S22, doi:10.1029/2007JD008956.

Zhu, J. H., S. W. Wang, X. D. Zhang, Q. Z. Mu, and Z. H. Xie, 2003: Basic modes of the general circulations under the global warming. *Prog. Nat. Sci.,* **13,** 417–421.